LIN, C. P., CHENG, K. T. & JOHNSON, W. R. (1975). *Phys. Rev. A*, **11**, 1946-1956.
PARKER, J. C. & PRATT, R. H. (1984). *Phys. Rev. A*, **29**, 152-158.
SCHAUPP, D., SCHUMACHER, M., SMEND, F., RULLHUSEN, P. & HUBBELL, J. H. (1983). *J. Phys. Chem. Ref. Data*, **12**, 467-512.
SCHUMACHER, M. & STOFFREGEN, A. (1977). *Z. Phys. A*, **283**, 15-19.
SMEND, F., SCHAUPP, D., CZERWINSKI, H., SCHUMACHER, M., MILLHOUSE, A. H. & KISSEL, L. (1987). *Phys. Rev. A*, **36**, 5189-5199.
SMITH, D. Y. (1987). *Phys. Rev. A*, **35**, 3381-3387.
TEMPLETON, D. H. (1962). In *International Tables for X-ray Crystallography*, Vol. III, edited by C. H. MACGILLAVRY & G. D. RIECK, p. 213. Birmingham: Kynoch Press. (Present distributor Kluwer Academic Publishers, Dordrecht.)
TEMPLETON, L. K. & TEMPLETON, D. H. (1988). *Acta Cryst.* A**44**, 1045-1051.
WANG, M. S. (1986). *Phys. Rev. A*, **34**, 636-637.
WANG, M. S. & CHIA, S.-H. (1988*a*). *Phys. Rev. A*, **38**, 1286-1288.
WANG, M. S. & CHIA, S.-H. (1988*b*). *Phys. Rev. A*, **37**, 2968-2969.
WANG, M. S. & CHIA, S.-H. (1988*c*). *Phys. Rev. A*, **38**, 5639-5641.
WANG, M. S. & PRATT, R. H. (1983). *Phys. Rev. A*, **28**, 3115-3116.

Acta Cryst. (1990). A**46**, 175-186

Small-Angle Techniques for the Asymptotic Analysis of X-ray Diffraction Peaks

BY S. CICCARIELLO*

Dipartimento di Fisica 'G. Galilei', via Marzolo 8, 35131 *Padova, Italy*

(*Received* 10 *April* 1989; *accepted* 13 *September* 1989)

Abstract

Any wide-angle X-ray scattering (WAXS) peak, relevant to a powder sample of crystallites with negligible internal disorder, is the Fourier transform of the so-called oriented stick probability function (oSPF) of the filled part of the sample, with the stick orientated along the reflexion direction. From this observation the following consequences are obtained: the correlation function used in small-angle X-ray scattering (SAXS) is the average of the former oSPF's over all possible stick orientations; any peak profile asymptotically vanishes as $S_r h^{-2}$, where S_r is the (specific) area of the interphase surface presented by the sample along the reflexion direction; oscillatory deviations, behaving as $S_{r,\|} \cos(hL) h^{-2}$, are present only when a subset (having area $S_{r,\|}$) of the interface, after having been translated by L along the reflexion direction, superposes on itself; the angularity of the interphase surface can be measured by a natural modification of the Porod integral relation. For samples really isotropic, the above quantities should not depend on the reflexion direction and thus they should be equal to those measured by SAXS experiments. These results are applied to three ideal isotropic powder samples made up, respectively, of monodisperse spherical, cubic and cylindrical crystallites as well as to the analysis of two WAXS peaks diffracted by two real samples of zirconia powders.

I. Introduction

The aim of this paper is to point out that many of the ideas used for analysing the asymptotic behaviour of small-angle X-ray scattered intensities (SAXS) can be usefully applied, *mutatis mutandis*, in the realm of wide-angle scattering (WAXS) in order to assess the behaviour of the peak intensities in the tail regions. Although the practical application of this method suffers two serious limitations, *i.e.* the powder samples must be made up of crystallites with negligible internal disorder and the measured WAXS peaks must not fall so close to each other as to make the observation of an asymptotic tail region impossible, the results of our analysis are interesting for two reasons: they allow one to appreciate the geometrical implications hidden in the functional forms usually assumed in best-fitting observed peaks and to unify the procedures used in interpreting small- and wide-angle experimental results.

The plan of the paper is the following. In the next section (§ II), the general theoretical expressions on which our analysis is based as well as the conditions for the samples we shall deal with will be written down. In § III, we shall discuss in detail the relationship between the WAXS peak profiles and the so-called oriented stick probability functions (oSPF). We also show how to obtain along the way the SAXS idealization of a sample. It turns out that the SAXS intensity is *essentially* the 000 WAXS reflexion and that the corresponding correlation function is the angular average of the aforesaid oSPF's. In this way it becomes clear that many of the techniques used for analysing SAXS intensities can be applied also to WAXS profiles. In § IV, some recent theoretical results relating the continuity properties of the derivatives of the oSPF's to some geometrical features of the crystallite boundaries will be recalled, while in § V we show how these continuity properties determine the asymptotic behaviour of WAXS profiles.

* Present address (until October 1990): Laboratoire de Physique des Solides, Bâtiment 510, 91405 Orsay CEDEX, France.

0108-7673/90/030175-12$03.00

The concluding section (§ VI) illustrates a preliminary application to two real samples and summarizes the results. In the Appendix, we give a detailed application of the results to the three simplest crystallite shapes: spherical, right circular cylindrical and cubic.

II. General definitions and assumptions

According to the general theory of X-ray scattering, the profiles of the peaks of the intensity [$\equiv I(\mathbf{h})$] of the radiation scattered by a powder sample are related both to the sizes of the constituent crystallites and to the disorder present in the lattices of the latter.* For the sake of simplicity we shall confine ourselves mainly to samples where disorder effects can be neglected. Under these assumptions, the electronic density of a single crystallite can be written as (Guinier, 1963)

$$\sum_{\mathbf{m}} \rho_{\text{cell}}(\mathbf{r}-\mathbf{r}_{\mathbf{m}})\rho_{V_{\text{fl}}}(\mathbf{r}_{\mathbf{m}}),$$

where $\rho_{\text{cell}}(\mathbf{r})$ is the electronic density of the unit cell and the sum is over all the cells whose representative points $\mathbf{r}_{\mathbf{m}}$ fall inside the spatial set V_{fl} filled by the crystallite. In fact, the function $\rho_{V_{\text{fl}}}(\mathbf{r})$, known as the form factor of the region filled by the crystallite, is defined as being equal to one or to zero depending on whether the tip of the vector $\mathbf{r}$ lies inside or outside V_{fl}, respectively. [For this reason, according to a more widespread definition, $\rho_V(\mathbf{r})$ represents the function characteristic of the set V.] In the case of a powder, one has crystallites with different orientations and with different shapes and/or dimensions. To allow them to be distinguished, they will be labelled by indices i and j. The latter refers to the orientation, while the former refers both to the size and to the shape. In this way, the electronic density of a crystallite powder sample, $\rho_e(\mathbf{r})$, can be written as

$$\rho_e(\mathbf{r}) = \sum_{\mathbf{m},j,i} \rho_{\text{cell},j}(\mathbf{r}-\mathbf{r}_{\mathbf{m},j})\rho_{V_{j,i}}(\mathbf{r}_{\mathbf{m},j}). \qquad (1)$$

The complication related to the different orientations of the unit cell inside the differently orientated crystallites has been accounted for by the fact that the electronic density of the cell $\rho_{\text{cell},j}(\mathbf{r})$ as well as the relevant vector positions $\mathbf{r}_{\mathbf{m},j}$ depend on j, the index which labels the angular orientation of the crystallite.* If one denotes by $\mathcal{R}_j^{-1}$ the rotation which transforms $\rho_{\text{cell}}(\mathbf{r})$ into $\rho_{\text{cell},j}(\mathbf{r})$, then

$$\rho_{\text{cell},j}(\mathbf{r}) = \rho_{\text{cell}}(\mathcal{R}_j\mathbf{r}) \qquad (2)$$

and a similar relation holds true for the vectors **a**, **b**, **c** defining the unit cells in the two cases. The amplitude of the scattered radiation is obtained by Fourier transforming (FT) (1) and reads

$$\begin{aligned} A(\mathbf{h}) &= \sum_{\mathbf{m},j,i} \tilde{\rho}_{\text{cell},j}(\mathbf{h})\tilde{\rho}_{V_{j,i}}(\mathbf{h}-\mathbf{Q}^*_{\mathbf{m},j})/V_c \\ &= \sum_{\mathbf{m},j,i} \tilde{\rho}_{\text{cell}}(\mathcal{R}_j\mathbf{h})\tilde{\rho}_{V_i}(\mathcal{R}_j\mathbf{h}-\mathbf{Q}^*_{\mathbf{m}})/V_c. \end{aligned} \qquad (3)$$

In (3), V_c is the volume of the unit cell, the tilde over a symbol denotes the FT, $\mathbf{Q}^*_{\mathbf{m}}$ is the vector associated with the $\mathbf{m}$ reflection in reciprocal space, while $\mathbf{Q}^*_{\mathbf{m},j}$ refers to the properly rotated reciprocal space.† The scattered intensity is the square modulus of the amplitude. Thus, from (3), after assuming that the sum of the crossed terms averages to zero, one gets

$$I(\mathbf{h}) = \sum_{\mathbf{m},j,i} \left| \frac{\tilde{\rho}_{\text{cell}}(\mathcal{R}_j\mathbf{h})}{V_c} \right|^2 |\tilde{\rho}_{V_i}(\mathcal{R}_j\mathbf{h}-\mathbf{Q}^*_{\mathbf{m}})|^2. \qquad (4)$$

III. Connection with SAXS theory

The expression for the small-angle X-ray scattered intensity as well as that for the wide-angle X-ray profiles follows immediately from the previous equation.

(*a*) *SAXS profile*

In this case, in fact, one has to refer to the reflexion $\mathbf{m} = 000$, *i.e.* $\mathbf{Q}^*_{\mathbf{m}} = 0$ and h has to be restricted to the region

$$h < \pi \min(a^*, b^*, c^*) \qquad (5)$$

so that it does not trespass on the next reflexion regions. In this situation, the sum over j amounts to averaging over the orientations of the particles having size i. If one assumes that the latter are quite numerous and isotropically distributed, the former average can be converted into an integral over all the possible

* In this paper we shall refer only to diffraction profiles which are the ideally measured ones. In other words, they are the profiles obtained from the experimentally measured ones after having applied all the corrections related to the finite size of the collimation slits, to the lack of monochromaticity of the beam and to unavoidable background effects. [See for instance Delhez, de Keijeser & Mittemeijer (1982) and Enzo, Fagherazzi, Benedetti & Polizzi (1988).]

* For notational simplicity, instead of $V_{\text{fl},i}$ we simply use $V_{j,i}$. Moreover, Ino & Minami (1979) have clearly shown that the definition of the electron density, as given by (1), has a certain degree of arbitrariness. This, however, can be safely neglected when crystallites contain more than, say, four or five unit cells per edge. On the contrary, for smaller crystallites, one expects that the atoms on the surface do not have their ideal crystalline positions. Consequently, neglecting disorder effects would appear to be a limitation more serious than the former ambiguity.

† Note that our $\mathbf{Q}^*_{\mathbf{m}}$'s are 2π times the standard ones, *i.e.* $\mathbf{Q}^*_{\mathbf{m}} = 2\pi(h\mathbf{a}^* + k\mathbf{b}^* + l\mathbf{c}^*)$, where $\mathbf{a}^*$, $\mathbf{b}^*$, $\mathbf{c}^*$ are the standard vectors defining the reciprocal-space unit cell. [See, *e.g.*, Guinier (1963), page 86, equation (4.11).]

orientations of **h** and one obtains

$$I_{SA}(h) = \int_{\Omega} d\hat{\omega} \sum_i \langle \mathcal{N}_i \rangle \left| \frac{\tilde{\rho}_{cell}(h\hat{\omega})}{V_c} \right|^2 |\tilde{\rho}_{V_i}(h\hat{\omega})|^2$$

$$= \left| \frac{\tilde{\rho}_{cell}(h\hat{\omega}_0)}{V_c} \right|^2 \int_{\Omega} d\hat{\omega} \sum_i \langle \mathcal{N}_i \rangle |\tilde{\rho}_{V_i}(h\hat{\omega})|^2, \quad (6)$$

where $\langle \mathcal{N}_i \rangle$ is the average number of the ith kind of particle per unit solid angle. In obtaining the last equality we have used the second theorem of the average for the integrals and thus $\hat{\omega}_0$ denotes the appropriate point. However, since h obeys condition (5) and $\tilde{\rho}_{cell}(\mathbf{h})$ is a slowly varying function in that region, one can reasonably put $\tilde{\rho}_{cell}(h\hat{\omega}_0) \simeq \tilde{\rho}_{cell}(0)$. This quantity is proportional to the number of electrons present in the unit cell ($\equiv N_{el}$) and thus the factor in front of the last integral in (6) can be reasonably approximated by

$$|\tilde{\rho}_{cell}(h\hat{\omega}_0)/V_c|^2 \simeq (eN_{el}/V_c)^2 \equiv \bar{n}^2, \quad (7)$$

where $\bar{n}$ represents the average electronic density of the filled part of the sample and e is the electron charge. The characteristic function of the total filled up region V_{Fl} is given by

$$\rho_{V_{Fl}}(\mathbf{r}) = \sum_{i,j} \rho_{V_{i,j}}(\mathbf{r}), \quad (8)$$

and the SAXS electronic density is

$$n(\mathbf{r}) = \bar{n}\rho_{V_{Fl}}(\mathbf{r}). \quad (9)$$

Then it is easy to check that the standard SAXS definition of the intensity

$$I_{SA}(h) = |\tilde{n}(\mathbf{h})|^2 = (4\pi)^{-1} \int_{\Omega} d\hat{\omega} |\tilde{n}(h\hat{\omega})|^2 \quad (10)$$

coincides with our previous expressions, *e.g.* (6) combined with (7). From (9), (10) can be written as the three-dimensional FT

$$I_{SA}(h) = \bar{n}^2 V_{Fl} \int_{R^3} dv \exp(i\mathbf{h} \cdot \mathbf{r}) \gamma(r) \quad (11)$$

of the so-called correlation function of the sample

$$\gamma(r) = \frac{1}{4\pi V_{Fl}} \int_{\Omega} d\hat{\omega} \int_{R^3} dv_1 \, \rho_{V_{Fl}}(\mathbf{r}_1 + \mathbf{r}\hat{\omega}) \rho_{V_{Fl}}(\mathbf{r}_1). \quad (12)$$

We have shown how and when (9) follows from (1) and given the conditions required for (10) to be equivalent to (4) around the 000 reflexion and this yields clearly a more unified presentation of the WAXS and SAXS theoretical formulations. The generalization required for dealing with samples, which require more than two phases from the point of view of a SAXS idealization, is trivially obtained by assuming that one has two or more different unit cells. Finally, one should also note that the hypothesis on the absence of disorder effects or, equivalently, on the assumed existence of well defined and replicated unit cells can be considerably weakened since the crucial approximations are the validity of (7) and that the ambiguity in drawing particle boundaries [see Ino & Minami (1979) and Ciccariello, Goodisman & Brumberger (1988)] can be neglected. These remarks should also clarify why SAXS idealizations are possible and indeed quite useful in the case of biological liquid solutions and, more generally, of amorphous systems.

(*b*) *WAXS profiles*

We turn now to the derivation of the expression of the peak profile relevant to a reflexion, labelled r and different from the 000 one. [See Guinier (1963), pp. 126–140.] At this point the assumption that crystallites, on average, are sufficiently large that $\rho_{V_i}(\mathbf{h})$ can be considered different from zero only when $h < \pi \min(a^*, b^*, c^*)$ plays a very important role. This implies that the light spots around the points of the reciprocal-space lattice are quite small. Consequently, the sum over all possible orientations j of the crystallites, required in (4), becomes equivalent to integration over the sets of those directions which ensure that **h** lies inside the spots which are around the considered reflexion and around the reflexions which can be obtained by rotations of the latter. The smallness of the spots allows us: (i) to approximate these sets by planar ones; (ii) to use the decomposition $\mathcal{R}_i\mathbf{h} = \mathbf{h}_\perp + \mathbf{Q}_r^* + h_\parallel \hat{\mathbf{s}}_{0r}$, where $\hat{\mathbf{s}}_{0r}$ is the unit vector specifying the direction of the reflexion $\mathbf{Q}_r^*$, $\mathbf{h}_\perp \cdot \hat{\mathbf{s}}_{0r} = 0$ and $h_\parallel = (\mathcal{R}_i\mathbf{h}) \cdot \hat{\mathbf{s}}_{0r} - Q_r^*$; and (iii) to put $\tilde{\rho}_{cell}(\mathcal{R}_j\mathbf{h}) \simeq \tilde{\rho}_{cell}(\mathbf{Q}_r^*)$. In this way, the powder profile around the rth Bragg reflexion will be

$$I_{WA,r}(h) = \sum_i{}' \left| \frac{\tilde{\rho}_{cell}(\mathbf{Q}_{r'}^*)}{Q_{r'}^* V_c} \right|^2 \langle \mathcal{N}_{i,r} \rangle \times \int d^2h_\perp |\tilde{\rho}_{V_i}(\mathbf{h}_\perp + h\hat{\mathbf{s}}_{0r'})|^2 \quad (13)$$

where we have substituted the standard symbol h for $h_\parallel$ and $\langle \mathcal{N}_{i,r} \rangle$ denotes the appropriate average number density of particles. The prime on the summation symbol reminds us that we have to sum over all the orientations $\hat{\mathbf{s}}_{0r'}$ of the reciprocal-lattice vectors $\mathbf{Q}_{\mathbf{m}}^*$, such that $Q_{\mathbf{m}}^* = Q_r^*$. Thus, the sum corresponds to an angular average, necessary in order to make the integral on the right-hand side of (13) independent of the choice of a particular orientation for particles having size i, implicitly assumed through the presence of V_i on the right-hand side of (13). In order to make the latter property more evident, one can substitute the sum over j for the primed sum and write

$$I_{WA,r}(h) = \mathscr{C} \sum_{i,j} \int d^2h_\perp |\tilde{\rho}_{V_{i,j}}(\mathbf{h}_\perp + h\hat{\mathbf{s}}_{0r})|^2, \quad (14)$$

where $\mathscr{C}$ is an appropriate normalization factor, to be specified later. If we recall once more the assumption that the sum of the crossed terms averages to zero, it is straightforward to convert (14) into

$$I_{\mathrm{WA},r}(h) = \mathscr{C} V_{\mathrm{Fl}} \int_{-\infty}^{\infty} \exp(iht)\gamma_r(t)\,\mathrm{d}t, \qquad (15)$$

where

$$\gamma_r(t) \equiv V_{\mathrm{Fl}}^{-1} \int_{R^3} \mathrm{d}v_1\, \rho_{V_{\mathrm{Fl}}}(\mathbf{r}_1 + t\hat{\mathbf{s}}_{0r})\rho_{V_{\mathrm{Fl}}}(\mathbf{r}_1). \qquad (16)$$

Equations (15) and (11), with the related definitions (16) and (12), are the starting point of the following discussion. On the one hand, they show that the SAXS correlation function (12) is the angular average of the oSPF's (16) evaluated with respect to all possible directions ($\hat{\mathbf{s}}_{0r}$). Clearly, if the isotropy is realized exactly, $\gamma_r(t)$ does not depend on the chosen direction $\hat{\mathbf{s}}_{0r}$ and then $\gamma_r(t)$ is independent of r and equal to $\gamma(t)$. On the other hand, the WAXS and SAXS profiles differ only because the first is a one-dimensional FT while the second is a three-dimensional one. We stress that this is the difference responsible for the different *asymptotic* behaviour of the two profiles, as will be clear later. One should also note that the difference has arisen from the peculiar position of the 000 reflexion. In fact, while for the reflexions with $r \neq 0$ it has been possible to convert the angular average infinitesimal measure $\mathrm{d}\omega$ into the planar one $\mathrm{d}\mathbf{h}_\perp / Q_r^{*2}$, for reflexion 000 this is clearly impossible. Using now the rotation invariance of $\gamma(r)$ as well as the parity properties of $\gamma_r(t)$, one can write (11) and (15) as

$$I_{\mathrm{SA}}(h) = (4\pi V_{\mathrm{Fl}}\bar{n}^2/h) \int_0^{\infty} t\gamma(t)\sin(ht)\,\mathrm{d}t \qquad (17)$$

$$I_{\mathrm{WA},r}(h) = 2\mathscr{C} V_{\mathrm{Fl}} \int_0^{\infty} \gamma_r(t)\cos(ht)\,\mathrm{d}t. \qquad (18)$$

Therefore, when the isotropy holds true, they are related through

$$I_{\mathrm{SA}}(h) = -(2\pi\bar{n}^2/\mathscr{C}h)\,\mathrm{d}[I_{\mathrm{WA},r}(h)]/\mathrm{d}h \qquad (18a)$$

and are different FT's of the same function, which can be obtained by using one of the following expressions

$$\gamma(t) = (\pi/4t\pi\bar{n}^2 V_{\mathrm{Fl}}) \int_0^{\infty} hI_{\mathrm{SA}}(h)\sin(ht)\,\mathrm{d}h \qquad (19)$$

$$\gamma_r(t) = (\pi/4\mathscr{C}V_{\mathrm{Fl}}) \int_0^{\infty} I_{\mathrm{WA},r}(h)\cos(ht)\,\mathrm{d}h, \qquad (20)$$

obtained by inverting integral transforms (17) and (18). Thus, in the case of exact isotropy, from (18a) any peak profile has to be a non-increasing h function and from (19) and (20) one could determine, at least in principle, $\gamma(t)$ by using only the measurements around one reflexion. In practice, things go differently and then, assuming that (19) and (20) are still valid, one can obtain quantitative information on anisotropies present in the sample. To this aim it is important to know:

(i) how geometrical features of crystallite boundaries, also referred to as the interphase boundary of the sample, determine the continuity properties as well as the values, at particular points, of the derivative of the oSPF's;

(ii) how the aforesaid properties can be obtained directly from observed peak profiles.

This task represents essentially the adaptation of well known SAXS techniques to the analysis of WAXS profiles. It will be performed by analysing point (i) in the next section and point (ii) in § V.

IV. Properties of $\gamma_r(t)$

Recalling that we are considering powder samples, let us call 1 the phase inside the sample crystallites and 2 the void one. Comparing (16) with the oSPF $\mathscr{P}_{1,1}(t\hat{\mathbf{s}}_{0r})$, defined by (II.8) in the paper by Ciccariello (1985), which will be referred to as I, one concludes that

$$\gamma_r(t) = \mathscr{P}_{1,1}(t\hat{\mathbf{s}}_{0r}). \qquad (21)$$

In this way the continuity properties of $\gamma_r(t)$ and of its derivatives will be those worked out in I for the oSPF's. Therefore, we shall recall the main results of I, illustrating them with some examples.

From definition (16) it is evident that $\gamma_r(t)$ is an even continuous non-negative function which becomes identically equal to zero as t becomes larger than the maximal extension of the sample in the direction $\hat{\mathbf{s}}_{0r}$ and thus the finiteness of the sample makes the support of $\gamma_r(t)$ compact.

(*a*) *First-order derivative*

From (16) and (21) one sees that $\gamma_r'(t)$, the first-order derivatives of $\gamma_r(t)$, can be obtained acting with the differential operator $\hat{\mathbf{s}}_{0r} \cdot \nabla$ on $\mathscr{P}_{1,1}(\mathbf{r})$ and then by putting $\mathbf{r} = t\hat{\mathbf{s}}_{0r}$. According to (I-III.3), the former derivative is equal to the projection along $\hat{\mathbf{s}}_{0r}$ of that part of the interphase boundary which lies inside the filled region of the sample, once the latter have been shifted by $\mathbf{r}$. Moreover, the discussion reported in § IV-1 of I has shown that:

(*a*) the first-order derivative of $\mathscr{P}_{1,1}(\mathbf{r})$, evaluated along a particular direction $\hat{\boldsymbol{\nu}}$, can have only finite discontinuities;

(*b*) these are present only for those $\mathbf{r}$ values such that the outset interphase surface and the $\mathbf{r}$-translated one superimpose at least in part;

(*c*) the value of the discontinuity is equal to the difference of the areas of the projections of the two surfaces which superpose as the limiting configuration is reached from the left or from the right. [See (I-IV.7).]

From this result immediately follows that the first-order derivative of any oSPF has a finite discontinuity at $\mathbf{r}=0$. In fact, one finds that the limit of $(\hat{\boldsymbol{\nu}}\cdot\nabla)\mathscr{P}_{1,1}(\hat{\boldsymbol{\nu}}r)$, as $r\to 0^+$, is equal to

$$\int_{\Sigma^{(-)}} [\hat{\boldsymbol{\nu}}\cdot\hat{n}(\mathbf{r})]\,\mathrm{d}S.$$

[Here $\hat{n}(\mathbf{r})$ is the unit vector orthogonal at $\mathbf{r}$ to the surface of the particle and pointing outwardly to the latter, while $\Sigma^{(-)}$ denotes the subset of the interphase boundary where the integrand is negative. In fact, owing to the previous orientation of $\hat{n}(\mathbf{r})$, only that subset contributes since, as $r\to 0^+$, it lies inside the particles.] On the contrary, the limit of $(\hat{\boldsymbol{\nu}}\cdot\nabla)\mathscr{P}_{1,1}(\hat{\boldsymbol{\nu}}r)$ as $r\to 0^-$ is just the opposite. Therefore, combining these results, one concludes that

$$\gamma_r'(0^+) = -\mathscr{S}_r \equiv -\sum_i S_{i,r}/V_{\mathrm{FI}}, \tag{22}$$

where the sum is performed over all the particles and $S_{i,r}$, defined as

$$S_{i,r} \equiv \int_{\Sigma_i^{(-)}} [\hat{\mathbf{s}}_{0r}\cdot\hat{n}(\mathbf{r})]\,\mathrm{d}S \tag{23}$$

is equal to half the area of the unfolded projection of the surface of particle i on a plane orthogonal to $\hat{\mathbf{s}}_{0r}$. Note that in order to evaluate the area we have to unfold the projection and that $\gamma_r'(0)$ is a negative quantity. Moreover, in the isotropic case, one can apply the argument proposed by Debye, Anderson & Brumberger (1957) and prove that

$$\mathscr{S}_r = S_T/4V_{\mathrm{FI}}, \tag{23a}$$

where S_T is the area of the total interphase surface.

If one assumes that particles have a strictly convex* shape and one recalls the assumption that overlapping of different particles, after sample translations, can be neglected, then one can show that $\gamma_r'(t)$ is non-positive (non-negative) for any positive (negative) t. In fact, under these assumptions, the expression of the oSPF

$$\gamma_r(t) = \int_{|t|}^{\infty} (M-|t|)\,\mathrm{d}\sigma_M/V_{\mathrm{FI}} \tag{24}$$

reported by Guinier (1963, p. 134) is correct. In (24), $\mathrm{d}\sigma_M$ is the area of the infinitesimal basis of the cylinder, having length M and the bases on the particle boundary, parallel to $\hat{\mathbf{s}}_{0r}$ and fully contained inside the particle. Clearly, only when the former hypotheses are fulfilled, does integral (24) yield correctly the oSPF expression. Taking the first-order derivative of (24), one gets

$$\gamma_r'(t) = -\mathrm{sign}\,(t)\int_{|t|}^{\infty} \mathrm{d}\sigma_M/V_{\mathrm{FI}}. \tag{25}$$

* We recall that a particle is convex when any segment, having its ends on the particle boundary, lies completely inside the particle. Examples of non-convex particles are innumerable, for instance L-shaped particles, hollow spheres, tori *etc.*

The positiveness of $\mathrm{d}\sigma_M$ ensures the validity of the aforesaid statement. In the Appendix we illustrate these results, discussing in detail the three simplest examples of crystallites, namely the spherical, the right circular cylindrical and the cubic ones.

(*b*) *Second-order derivative*

We shall now discuss the properties of $\gamma_r''(t)$, *i.e.* the second-order derivative of the oSPF.

When the conditions required for the validity of (24) are fulfilled, taking the derivative of (24) and putting $\mathrm{d}\sigma_M = g(M)\,\mathrm{d}M$ one gets

$$\gamma_r''(t) = g(|t|). \tag{26}$$

This shows that, under the previous assumptions, $\gamma_r''(t)$ is a non-negative quantity, since $g(M)$ is non-negative.

We recall that according to the discussion reported in § III.2 of I, based on assumptions more general than the ones required just above, $\gamma_r''(t)$ is given by the integral of a suitable function along the curve resulting from the intersection of the outset sample interface with the one resulting from the shift of the sample by $t\hat{\mathbf{s}}_{0r}$. [See equation (I-III.4).] Stemming from this expression, it has been shown that the second-order derivative, besides the δ-like singularities arising from the finite discontinuities pointed out above, is discontinuous at those t values where one of the following two conditions takes place:

(i) one of the sharp edges, eventually present on the particles' surface, superimposes (at least in part) on the surface resulting from the translation by $t\hat{\mathbf{s}}_{0r}$;

(ii) the translated surface is tangent at some point of the original surface and the tangent plane is orthogonal to the translation direction. In this case it can happen that the two surfaces, in the neighbourhood of the contact point, have in common only this point, or that they intersect each other along two lines meeting at that point or, finally, that they touch each other along one line. In the three cases one speaks respectively of elliptic, hyperbolic and parabolic contact point.

The general expressions of the discontinuities relevant to cases (i) and (ii) are given essentially by equations (I-*B*.5) and (I-*A*.16), provided one puts $\hat{\boldsymbol{\mu}} = \hat{\boldsymbol{\nu}} = \hat{\boldsymbol{\omega}} = \hat{\mathbf{s}}_{0r}$ and $\mathbf{r} = t\hat{\mathbf{s}}_{0r}$. In fact, taking properly into accout all the factors, in the first case one finds

$$V_{\mathrm{FI}}[\gamma_r''(t^+) - \gamma_r''(t^-)] = -\int_{\Gamma} \left\{\left[\frac{(\hat{\boldsymbol{\sigma}}\cdot\hat{\mathbf{s}}_{0r})(\hat{\boldsymbol{\sigma}}'\cdot\hat{\mathbf{s}}_{0r})}{\sin\beta}\right]^{+} - \left[\ldots\right]^{-}\right\} \mathrm{d}l. \tag{27}$$

The integral is performed along that part Γ of the edge which superposes on the particle boundary once the latter have been translated by $r\hat{\mathbf{s}}_{0r}$, $\hat{\boldsymbol{\sigma}}$ and $\hat{\boldsymbol{\sigma}}'$ are

the normal to the initial and to the translated surface which meet along the considered edge, while β, with $0<\beta<\pi$, is the dihedral angle between the two surfaces at the edge point parameterized by the curvilinear coordinate l. Finally, the upper indices + and − account for the fact that the quantities inside square brackets generally change as we approach the limit from the right or from the left, respectively.*

In the second case and for elliptical contact points one finds

$$V_{\mathrm{FI}}[\gamma_r''(t^+)-\gamma_r''(t^-)]=2\pi\ \mathrm{sign}\ (F)(\hat{\boldsymbol{\sigma}}\,.\,\hat{\boldsymbol{\sigma}}')\mathscr{K}_G^{-1/2}(t). \tag{28}$$

Here $\mathscr{K}_G(t)$ is the Gaussian curvature (Ciccariello, 1989) of the surface obtained by considering the distance of the two meeting surfaces along straight lines parallel to $\hat{\mathbf{s}}_{0r}$ or, equivalently, to the line orthogonal to the surfaces at the contact point. Moreover, sign (F) denotes the sign of the difference surface in a sufficiently small neighbourhood of the contact point. Therefore, it is positive or negative depending on whether the translated surface falls externally or internally to the original surface in the neighbourhood of the contact point.†

Before closing this section we think it worthwhile to discuss briefly another important geometrical parameter of samples, the *angularity*. This quantity roughly speaking measures the number of edges present on the sample interface. It was first introduced by Porod (1965) and measured by Tchoubar & Méring (1969). Subsequently, it has been thoroughly discussed and used for analysing the behaviour of some catalysts by Ciccariello & Benedetti (1985). Mathematically, the angularity can be defined as the $\gamma_r''(0^+)$ value, *i.e.* as the limiting value of $\gamma_r''(t)$ as $t\to 0^+$. Indeed, starting from equation (I-III.11) with $i=j=1$, $\hat{\boldsymbol{\mu}}=\hat{\boldsymbol{\nu}}=\hat{\mathbf{s}}_{0r}$ and $\mathbf{r}=t\hat{\mathbf{s}}_{0r}$ and using equations (I-*A*.2) and (I-*B*.4), one finds that in the case of an edge $\gamma_r''(0^+)$ is given by (I-*B*.5), which is an integral of a known function along the edge. Similarly, the contribution of a contact point to $\gamma_r''(0^+)$ can be obtained from equation (I-*A*.15). Finally the proof that $\gamma_r''(0^+)=0$ in the case of a smooth surface, *i.e.* a surface such that at each of its points a uniquely oriented tangent plane exists, can be easily obtained noting that the intersection of this regular surface with its image translated by $t\hat{\mathbf{s}}_{0r}$ tends, as $t\to 0^+$, to an extremal curve, *i.e.* a curve such that at each of its points the unit vector $\hat{\boldsymbol{\sigma}}_1$, orthogonal to the surface on which the curve lies, is also orthogonal to the translation direction, *i.e.* $\hat{\boldsymbol{\sigma}}_1\,.\,\hat{\mathbf{s}}_{0r}=0$. These results clarify the reason why one refers to the $\gamma_r''(0^+)$ value as to the angularity of the sample. Finally we mention that using the aforesaid results one can show that the angularity value is always non-negative.*

V. Asymptotic analysis

The former quantities, at least in principle, can be measured starting from the measured peak profile.

The parity of $\gamma_r(t)$ allows one to write (15) as

$$I_{\mathrm{WA},r}(h)/2=\int_0^L \cos(ht)\gamma_r(t)\,\mathrm{d}t, \tag{29}$$

where L denotes the right extremum of the support of $\gamma_r(t)$. An integration by parts yields

$$I_{\mathrm{WA},r}(h)/2=-\sum_{m=1}^{p}\int_{l_m}^{L_m}[\sin(ht)/h]\gamma_r'(t)\,\mathrm{d}t$$

$$\equiv -\fint_0^L[\sin(ht)/h]\gamma_r'(t)\,\mathrm{d}t, \tag{29a}$$

where the initial integration interval $[0, L]$ is broken into p intervals, $[l_m, L_m]$, $m=1,\ldots,p$, in order to guarantee the continuity of the integrand inside each of them. In this way, $l_1=0$, $L_p=L$, $l_m=L_{m-1}$, $\gamma_r'(l_m^+)\neq\gamma_r'(L_{m-1}^-)$, $m=2,\ldots,p-1$ and the aforesaid prescription for the evaluation of integrals is made evident by the slash on the integral symbol as in (29*a*). Integrating once more by parts, one gets

$$I_{\mathrm{WA},r}(h)/2=-\sum_{m=0}^{p}[\cos(hL_m)/h^2]\gamma_{r,\Delta}'(L_m)$$

$$-\fint_0^L[\cos(ht)/h^2]\gamma_r''(t)\,\mathrm{d}t. \tag{30}$$

Here, according to the following definition,

$$\gamma_{r,\Delta}'(L_m)\equiv\gamma_r'(l_{m+1}^+)-\gamma_r'(L_m^-),\quad m=0,\ldots,p. \tag{31}$$

$\gamma_{r,\Delta}'(L_m)$ denotes the discontinuity value at the mth discontinuity point. This definition applies to the cases $m=0$ and $m=p$ by using the definitions $\gamma_r'(l_{p+1}^+)\equiv 0$ and $\gamma_r'(L_0^-)\equiv 0$ naturally suggested by the support properties of $\gamma_r(t)$. Recalling the result (22) and that the integral on the r.h.s. of (30) decreases faster than h^{-2}, one concludes that the leading asymptotic term of a single peak profile is

$$I_{r,\mathrm{asym}}(h)=\frac{2\mathscr{S}_r}{h^2}-2\sum_{m=1}^{p}\frac{\cos(hL_m)}{h^2}\gamma_{r,\Delta}'(L_m). \tag{32}$$

This expression looks similar to the leading

* In equation (I-*B*.5) this fact was accounted for by the characteristic set function $\rho_\Omega(\hat{\boldsymbol{\omega}})$.

† In passing we note that for hyperbolic and parabolic contact points (28) cannot be applied and this is clearly signalled by the fact that it becomes meaningless, since $\mathscr{K}_G(r)$ is negative or null in the two cases. These singular behaviours indicate that, in the asymptotic expansion of the intensity, we have to expect contributions which, albeit decreasing as h^{-3}, have an oscillatory factor different from the sine function or contributions which decrease as $h^{-\alpha}$, with $2<\alpha<3$ (Jones & Kline, 1958).

* More details on the way the angularity is related to the aforesaid geometrical features can be found in Ciccariello & Benedetti (1985) for the SAXS case, while in the Appendix we illustrate how the angularity works in some WAXS cases.

asymptotic term of the SAXS intensity. Some differences, however, are worth noting. In the latter case, in fact, the decrease is $O(h^{-4})$ (we are concerned with pin-hole geometry) and, moreover, the coefficients in front of the oscillatory terms are related to the discontinuities of the second-order derivative. Besides, oscillatory contributions proportional to the sine functions are expected when the discontinuities arise from hyperbolic contact points (Ciccariello, 1989). However, these differences can be considered as secondary ones, since they do not prevent the application of the general SAXS technique of analysis, which allows one to measure the aforesaid geometrical parameters stemming from the measured intensity. Multiplying by h^2 the observed peak profile, according to (32), at large h one should observe some wiggles, represented by the contribution $2\sum_{m=1}^{p}\cos(hL_m)\gamma'_{r,\Delta}(L_m)$, around the straight horizontal line, at height $2\mathscr{S}_r$, in the $[h, h^2 I_{\mathrm{WA},r}(h)]$ plane. In principle, this procedure allows one to measure the surface offered by the crystallite along the view direction $\hat{\mathbf{s}}_{0r}$, the fraction of the crystallite surfaces which are *parallel* as well as, through the frequency factor related to L_m, their relative distances. Of course this procedure works only when sample particles are to a good approximation monodisperse and have a shape sufficiently simple that only one or two oscillatory terms are required on the right-hand side of (32). On theoretical grounds, however, (32) is interesting because it shows that peak profiles asymptotically* decrease as h^{-2}. We recall that Allegra (1982) has already obtained this result, using however the so-called sampling-line method and rather general particle distribution. On the contrary, our derivation uses the property that any oSPF has a finite discontinuity at $t=0$ in consequence of the fact that crystallites have sharply defined boundaries, which is our only strong assumption.† Clearly this assumption is implicitly present in the sampling-line method, used by Allegra, so it is likely that the rest of his assumptions are equivalent to the assumed existence of a finite $\mathscr{S}_r$ value.

Once we have achieved by the previous analysis an accurate determination of the leading asymptotic term of $I_{\mathrm{WA},r}(h)$, it is also possible to measure $\gamma''_r(0^+)$, *i.e.* the angularity presented by the particle along the direction $\hat{\mathbf{s}}_{0r}$. In fact, subtracting from the peak profile its asymptotic leading term and multiplying by h^2 one is left on the r.h.s. of (30) with a cosine transform, which can be immediately inverted. One finds

$$\gamma''_r(t)=(1/\pi)\int_0^{\infty}\left[2\mathscr{S}_r-2\sum_{m=1}^{p}\cos(hL_m)\gamma'_{r,\Delta}(L_m)-h^2 I_{\mathrm{WA},r}(h)\right]\cos(ht)\,\mathrm{d}h. \tag{33}$$

The $t\to 0^+$ limit of (33) gives

$$\gamma''_r(0^+)=(1/\pi)\int_0^{\infty}\left[2\mathscr{S}_r-2\sum_{m=1}^{p}\cos(hL_m)\gamma'_{r,\Delta}(L_m)-h^2 I_{\mathrm{WA},r}(h)\right]\mathrm{d}h. \tag{34}$$

If one forgets for a moment the oscillatory contributions, the r.h.s. of (34) represents the algebraic value of the area delimited by the Porod plateau (*i.e.* the horizontal line $2\mathscr{S}_r$), and by the properly scaled intensity curve, *i.e.* $h^2 I_{\mathrm{WA},r}(h)$. Thus, quite similarly to the result first obtained by Porod (1965), the angularity of the particle along the direction $\hat{\mathbf{s}}_{0r}$ is proportional to the aforesaid area. From this point of view, (34) represents the generalization of Porod's result appropriate to WAXS profiles. Moreover, it shows also how the Porod sum rule has to be formulated when oscillatory contributions are present. For later convenience, in order to study how quickly the exact angularity value can be obtained from the integral on the right-hand side of (34) it is convenient to introduce the quantity

$$\Gamma_r(X)\equiv(1/\pi)\int_0^{X}\left[2\mathscr{S}_r-2\sum_{m=1}^{p}\cos(hL_m)\gamma'_{r,\Delta}(L_m)-h^2 I_{\mathrm{WA},r}(h)\right]\mathrm{d}h, \tag{35a}$$

which represents the value of the former integral truncated at $h=X$. Then one has

$$\gamma''_r(0^+)=\lim_{X\to\infty}\Gamma_r(X). \tag{35b}$$

VI. Concluding remarks

In our analysis we have emphasized the relation existing between oSPF's and peak profiles [see (15) and (16)] and pointed out the possibility of performing a SAXS-like analysis around WAXS peaks.

An immediate consequence of the first point is that parameterizations of peak profiles must involve functions decreasing as h^{-2}. This implies that their FT's must have a discontinuous derivative at $t=0$. Recalling that in the direct space the Lorentzian and the Voigt functions have respectively the following expressions: $\exp(-\alpha|t|)$ and $\exp(-\alpha|t|-\beta t^2)$ (Delhez *et al.*, 1982; Enzo *et al.*, 1988), one immediately realizes that in the reciprocal space they have the correct asymptotic behaviour, while this does not

* For a thorough discussion on the asymptotic condition as well as on its meaning we refer to Ciccariello, Goodisman & Brumberger (1988).

† We note that having neglected, in the calculation of $\gamma_r(t)$, the overlapping among different particles does not modify (22), since at very small t's overlapping of each particle with itself is the dominant effect. Possible exceptions, however, could be expected when the fractal dimension (Bale & Schmidt, 1984) of the sample interface is larger than two. In these cases $\mathscr{S}_r$ turns out to be divergent and the profile should decrease as $h^{-\alpha}$ with $\alpha<2$.

happen for the Gaussian parameterization: $\exp(-\beta t^2)$.

The natural question is whether it is really possible to measure quantities, usually obtained by SAXS intensities, using WAXS peaks. Obviously, the possibility is related to the peak separation. Indeed, when a peak is sufficiently well separated, the analysis is possible. Before concluding the paper we would like to sketch the results we have obtained by analysing the WAXS intensities diffracted by two powder samples of metastable cubic zirconia illustrated in the paper by Benedetti, Fagherazzi, Pinna & Polizzi (1990), to which we refer for the physical characterization of the samples. We have analysed the peaks 111 and 200, present in the two diffractograms shown at the bottom of Fig. 2 of that paper and relevant to the samples A_1 and A_2 of the previous authors (see their Table 2). Their broadening and their angular positions in fact are, respectively, large and low enough that one can reasonably neglect instrumental aberrations.*

The best-fit analysis has been performed using for the intensity the expression reported on the right-hand side of (32), confining ourselves to the case of a single oscillatory contribution. Besides, similarly to the SAXS case (Luzzati, Witz & Nicolaieff, 1961), we have added to this expression a constant contribution $\mathcal{B}$, to account for background effects and for possible deviations from the idealization discussed in § III, particularly that related to the assumption of a constant $\tilde{\rho}_{\text{cell}}$ value throughout the explored h range. For each peak, six different optimization runs have been performed. In fact, we have considered three different asymptotic h sets: $-0{\cdot}12 \le h \le -0{\cdot}06$, $0{\cdot}06 \le h \le 0{\cdot}12$ Å^{-1} and their union. In each of these sets we made two optimization runs. In the first, we assumed that no oscillation was present and thus we used as free parameters only $\mathcal{S}_r$ and $\mathcal{B}$, while in the second we used four parameters: $\mathcal{S}_r$, $\mathcal{B}$, L and $\gamma'_{r,\Delta}(L)$. Each peak profile has been normalized requiring that

$$\int_{-\infty}^{\infty} I_{\text{WA},r}(h)\, \mathrm{d}h = 2\pi$$

since $\gamma_r(0) = 1$.

In all cases we have found that no oscillatory contribution is required since the $\gamma'_{r,\Delta}(L)$'s have turned out quite small, while significant values for $\mathcal{S}_r$ and $\mathcal{A}_r \equiv \gamma''_r(0^+)$ have been obtained. (Their units are Å^{-1} and Å^{-2}, respectively.) Moreover, $\mathcal{S}_r$ appeared rather insensitive both to the parameterization used and on the chosen h interval. In Table 1 we report the reciprocal of the value obtained by averaging the ones relevant to the different runs. The reported error has been simply identified with the largest (absolute value) difference. The angularity $\mathcal{A}_r$ does not look so stable, as one can see from the value of the corresponding error shown in the table. For each sample, one sees that, apart from a few %, $\mathcal{S}_r^{-1}$ is independent of r, as one would expect when the powder sample is really isotropic. The independence of $\mathcal{A}_r$ on r is verified with an error of ~30% for sample A_2. Recalling that the angularity is a parameter much more difficult to measure, we would conclude that the isotropy is well verified. Comparing now the results relevant to the two samples, one sees that the average dimension of A_2 is larger than that of A_1 by a factor ~1·5. Also, the angularity of the latter sample is larger than that of the former. If one assumes that the dihedral angles among particle faces are constant, the previous result can be intuitively justified noting that the total length of the edges will be longer when a given volume is filled with smaller particles. Since the quantities $\mathcal{S}_r = S_r/4V_{\text{Fl}}$ differ by an unknown numerical factor from the corresponding quantities obtained from SAXS intensities by the Fedorova & Schmidt (1978) method, from the comparison of our results with the corresponding ones reported by Benedetti *et al.* (1990) in their Table 2, we can only say that the two pictures look rather similar. In particular, the ratio of their SAXS values (~2) is rather close to ours (~1·5). Thus, one can conclude that it is possible to measure some quantities, usually determined by SAXS experiments, by analysing the tail of a well separated WAXS peak.

Table 1. *The results of the best fits of the* 111 *and* 200 *peaks scattered by the samples* A_1 *and* A_2 *of zirconia powders, analysed by Benedetti et al.* (1990)

		$\mathcal{S}^{-1}$	$\mathcal{A}$	$\mathcal{B}$
A_1	(111)	38 ± 2	0·9 ± 0·4	245 ± 25
	(200)	40 ± 2	1·0 ± 0·5	257 ± 50
A_2	(111)	64 ± 6	0·3 ± 0·1	212 ± 20
	(200)	56 ± 4	0·4 ± 0·2	205 ± 30

In columns 3, 4 and 5 are reported the reciprocal specific surface (Å), the angularity (Å^{-2}) and the subtracted background. The values are the averages of the ones resulting from the six best-fit runs (see § VI). Similarly, in each of the reported cases the error is the largest difference of best-fit results from the average value. Finally, the SAXS average particle sizes obtained by Benedetti *et al.* (1990) with the Fedorova & Schmidt (1978) method are 7·1 and 15·1 nm for samples A_1 and A_2, respectively.

Stimulating and clarifying discussions with Professor G. Fagherazzi and with Drs S. Polizzi and M. Battagliarin as well as useful correspondence with Dr A. Benedetti are gratefully acknowledged. Financial support from the Italian Ministry of University and Scientific Research through 40% funds is gratefully acknowledged too.

* I am particularly grateful to Professor G. Fagherazzi for his suggestion of analysing these peaks and for having kindly supplied the experimental data.

APPENDIX

(a) *Spherical particle*

Stemming from definition (16) it is simple to evaluate the oSPF relevant to a spherical particle of diameter D. In fact the volume shared by the particle and the one translated by $t\hat{\mathbf{s}}_{0r}$, whatever $\hat{\mathbf{s}}_{0r}$, is $V[1-3|t|/2D+|t|^3/2D^3]$, where V denotes the volume of the sphere. Thus, one gets

$$\gamma_{sph}(t) = 1-3|t|/2D+|t|^3/2D^3 \quad |t| \le D$$
$$= 0 \quad |t| \ge D. \qquad (A.1)$$

According to our general discussion, since the sphere does not have finite subsets which are parallel, $\gamma'_{sph}(t)$ has to be continuous except at $t=0$. According to (22), in order to obtain the value of $\gamma'_{sph}(0^+)$ we need to know the area of the surface S_r offered by the sphere when it is observed along a particular direction. This value is simply $\pi D^2/4$. Thus,

$$\gamma'_{sph}(0^+) = -\pi D^2/4V = -3/2D \qquad (A.2)$$

as one can easily check by taking the derivative of (A.1).

The second-order derivative of $\gamma_{sph}(t)$ will have a discontinuity only at $t=D$, since the sphere has no edges and the contact condition takes place only when the sphere is shifted by D. Besides, the contact is elliptical and thus the discontinuity is finite.* On the other hand, the smoothness of the surface guarantees that $\gamma''_{sph}(0^+)$ is null. By explicit calculations, starting from (A.1), one finds

$$\gamma''_{sph}(0^+) = 0 \qquad (A.3)$$

$$\gamma''_{sph}(D^+) - \gamma''_{sph}(D^-) = -3/D^2. \qquad (A.4)$$

From (32) we deduce that the leading asymptotic term of the peak profile will be S_r/Vh^2. This result can be immediately checked evaluating the peak profile by Fourier transforming (A.1). One gets

$$I_{WA,sph}(h) = 2S_r/Vh^2 - [6D/(hD)^3] \times \{\sin(hD) - [1-\cos(hD)]/hD\}. \qquad (A.5)$$

From (A.5), it is easy to check, by a simple integration by parts of the second term, that the corresponding integral on the r.h.s. of (34) is equal to zero, as (A.3) predicts. Finally, Fig. 1 shows the Porod plateau and allows one to get a rough estimate of the lowest limit of the asymptotic region. This in fact appears to lie beyond the value $hD \simeq 2\pi$.

* In fact, choosing the z axis along $\hat{\mathbf{s}}_{0r}$, the difference surface between the two tangent spheres with their centres at (0, 0, 0) and (0, 0, D) is $F(x,y) = D - 2(D^2/4 - x^2 - y^2)^{1/2}$. Thus, around the contact point sign $(F) = 1$, the Gauss curvature is $16/D^2$ and $\hat{\boldsymbol{\sigma}} \cdot \hat{\boldsymbol{\sigma}}' = -1$. From (28) the value of the discontinuity at $t = D$ will be $\gamma''_{sph,\Delta}(D) = -3/D^2$.

(b) *Right circular cylindrical particle*

As will appear clear from the following discussion, the case of the cylindrical particle is deeper than the preceding one. The correlation function in fact depends on the observation direction $\hat{\mathbf{s}}_{0r}$. We have found it convenient to choose the reference system with the z axis along the cylinder axis and the origin at the centre of the lower base of the cylinder. The latter's height, diameter and volume are denoted by H, D and V. We shall denote by θ the angle formed by $\hat{\mathbf{s}}_{0r}$ with the z axis. The symmetry of the particle around the z axis will make $\gamma_{r,cyl}(t, \theta)$, the oSPF of the cylinder, dependent only on t and θ. The latter in particular will vary in the interval $[0, \pi]$. In order to evaluate $\gamma_{r,cyl}(t, \theta)$, we note that the cylinder translated by $t\hat{\mathbf{s}}_{0r}$ and the outset cylinder in general will share a right cylinder having height equal to $H - |t\cos\theta|$ and base equal to the set common to two

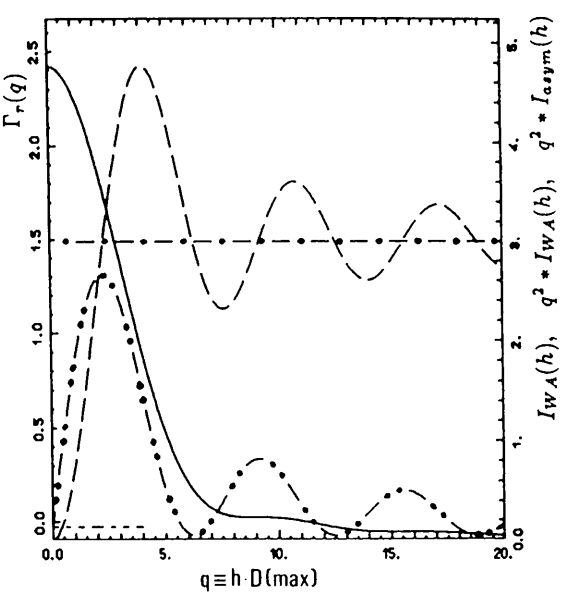

Fig. 1. The continuous line shows the peak profile $I_{WA,sph}(h)$, given by equation (A.5) relevant to a sphere with diameter D, while the dashed curve represents its wide-angle Porod plot, *i.e.* the plot of the function $q^2 I_{WA,sph}(h)$, with $q \equiv hD$. The horizontal dashed-dotted line is the plot of $q^2 I_{r,asym}(h)$ which, from equations (32) and (A.5), reduces to the constant value $2S_r D^2/V$. One should note how the dashed curve approaches the latter as h increases. The double-dotted dashed line represents the function $\Gamma_{r,sph}(q)$ obtained from evaluating numerically the function defined by (35a). One sees that as q increases $\Gamma_{r,sph}(q)$ approaches zero, although very slowly. Therefore the angularity, particularly in the case of a null value, is a quantity rather difficult to evaluate. In fact, setting the border of the asymptotic region at $q = 2\pi$, the relative error on the specific surface is smaller than 20%, while the absolute error on the angularity can be considerably larger. Note that, throughout the figures, the units for the vertical left and right scales are respectively D_{max}^{-2} and D_{max}, and that D_{max} denotes the length of the longest stick which has the reflexion orientation and lies completely inside the particle. However, for the peak profile, a further scale factor must be considered. In this case it is $0{\cdot}75D/4{\cdot}82$.

circles with diameter D with their centres set apart by a distance $x = |t| \sin\theta$. The area of this set is given by $2(D/2)^2\mathcal{S}(|t| \sin\theta/D)$ (Miller & Schmidt, 1962) with $\mathcal{S}(x)$ defined as

$$\mathcal{S}(x) = \arccos x - x(1-x^2)^{1/2}. \qquad (A.6)$$

Then the oSPF required is

$$\gamma_{r,\mathrm{cyl}}(t,\theta) = \begin{cases} (2/\pi)(1-|t\cos\theta|/H)\mathcal{S}(|t|\sin\theta/D) \\ \quad \text{if } 0 \le |t| \le D_{\max} \\ 0 \quad \text{elsewhere,} \end{cases} \qquad (A.7)$$

where

$$D_{\max} \equiv \min(D/\sin\theta, H/|\cos\theta|). \qquad (A.7a)$$

The continuity of $\gamma_{r,\mathrm{cyl}}(t,\theta)$ is evident. Besides, $\gamma_{r,\mathrm{cyl}}(t,\theta)$ is symmetric with respect to the exchanges $\theta \leftrightarrow \pi - \theta$ and $t \leftrightarrow -t$. For this reason, in order to simplify the notation, from now on the variables will be confined to the region $0 \le \theta \le \pi/2$, $t \ge 0$.

In order to find $\gamma'_{r,\mathrm{cyl}}(0^+,\theta)$, according to (22) we need to know the area of the cross section of the cylinder along the direction $\hat{\mathbf{s}}_{0r}$. This is clearly $DH\sin\theta + \pi(D/2)^2\cos\theta$ and thus

$$\gamma'_{r,\mathrm{cyl}}(0^+,\theta) = -[DH\sin\theta + \pi(D/2)^2\cos\theta]/V. \qquad (A.8)$$

Since for some translations the cylinder boundary superposes partly on itself, we have to expect finite discontinuities in $\gamma'_{r,\mathrm{cyl}}(t,\theta)$. The translations responsible for this phenomenon are the ones yielding a partial superposition of the bases. Therefore, they are characterized by the condition

$$t\cos\theta = H \quad \text{and} \quad \theta \le \theta_0 \equiv \arctan(D/H). \qquad (A.9)$$

The latter constraint in (A.9) is necessary because only the values of t slightly smaller than $H\sin\theta$ yield a finite intersection volume. The discontinuity value, according to the result of I (see § III.1), will be proportional to the difference of the projections of the areas which superpose as the limiting configurations are reached from the right and from the left, respectively. In our case, the limit from the right is zero, while the limit from the left is the area shared by two circles with their centres at a relative distance $t\sin\theta$, *i.e.* $2(D/2)^2\mathcal{S}(t\sin\theta)$. Thus, the expected discontinuity is

$$\gamma'_{r,\mathrm{cyl},\Delta}(H/\cos\theta,\theta) = 2(D/2)^2\mathcal{S}[(H/D)\tan\theta]\cos\theta/V, \quad \theta \le \theta_0. \qquad (A.10)$$

On the contrary, when $\theta \ge \theta_0$ no discontinuity exists. In this case, in fact, the possible tangency of the cylinders takes place only along a segment. The explicit derivation of (A.7) gives

$$\gamma'_{r,\mathrm{cyl}}(t,\theta) = \begin{cases} -(2/\pi)\mathcal{S}_1(t,\theta) & \text{when } 0 \le t \le D_{\max} \\ 0 & \text{elsewhere,} \end{cases} \qquad (A.11)$$

where

$$y \equiv \sin\theta/D$$

$$\mathcal{S}_1(t,\theta) \equiv \{\cos\theta\mathcal{S}(ty)/H + 2(1-t\cos\theta/H)y[1-(ty)^2]^{1/2}\}. \qquad (A.11a)$$

From this expression it is simple to check the validity of (A.9) and (A.10).

We turn now to the analysis of the second-order derivative. Since the cylinder has (two circular) sharp edges, the limit of $\gamma''_{r,\mathrm{cyl}}(t,\theta)$, as $t \to 0^+$ is different from zero and we have generally to expect an angularity different from zero.* Moreover, $\gamma''_{r,\mathrm{cyl}}(t,\theta)$ will be discontinuous for those t values such that the corresponding translations yield edges lying partly on the cylinder surface or a tangency condition at points where the touching surfaces are smooth. The first condition is realized when condition (A.9) is fulfilled. In this case we have a finite discontinuity.† The second condition is realized when the tangency takes place along one of the cylinder generatrices, *i.e.* when

$$t\sin\theta = D \quad \text{and} \quad \theta \ge \theta_0 \equiv \arctan(D/H). \qquad (A.12)$$

In this case the contacts are parabolic and the discontinuity is a divergence. By explicit calculations one finds that

$$\gamma''_{r,\mathrm{cyl}}(t,\theta) = \begin{cases} (4\sin\theta/\pi D)\mathcal{S}_2(t,\theta) & \text{when } 0 \le t \le D_{\max} \\ 0 & \text{elsewhere,} \end{cases} \qquad (A.13)$$

---

* From (27) it is rather easy to evaluate the limit value. As $t \to 0^+$, one sees that the top basis of the fixed cylinder cuts the lateral surface of the translated cylinder along an arc, which approaches a half-circumference. Similarly, the bottom basis of the translated cylinder cuts the lateral surface of the fixed cylinder along an arc which, neglecting its different altitude, is opposite to the former one. In both cases the dihedral angle is $\beta = \pi/2$, and the product of the scalar products, although each factor changes its sign, is equal to $-\cos\theta\sin\theta\cos\varphi$. φ denotes the angle between the normal to the lateral surface of the cylinder at a point on the edge and the projection of $\hat{\mathbf{s}}_{0r}$ on the plane of the basis. The y axis has been chosen along this direction, thus the integral along the top half-circumference will correspond to φ's in the interval $[-\pi/2, \pi/2]$. The integral is immediately performed and one finds that each half-circumference contributes $2[D/2\sin\theta\cos\theta/(\pi HD^2/4)]$. In this way, one finds that $\gamma''_r(0^+) = 2D\sin\theta\cos\theta/(\pi HD^2/4)$. [See (A.14).]

† The calculation of the discontinuity can be done along the same lines expounded in the preceding footnote. One has simply to note that the limiting top half-circumference is now the arc of the translated basis internal to the fixed top basis. Accordingly, φ will now range in the interval $[-\arccos(x/D), \arccos(x/D)]$, having denoted by $x = t\sin\theta$ the distance between the centres of the two upper bases. Performing the integral with respect to φ and noting that the overlapping limiting edges exist only when one considers the limit from below, one gets $\gamma''_{r,\Delta}(H/\cos\theta) = -2D\sin[ar\cos(H\tan\theta/D)]\sin\theta\cos\theta/(\pi HD^2/4)$ [see (A.15)].

where y is defined by the first of (A.11a) and

$$\mathcal{S}_2(t,\theta)\equiv\{(2\cos\theta/H)[1-(ty)^2]^{1/2} + ty^2(1-t\cos\theta/H)/[1-(ty)^2]^{1/2}\}. \quad (A.13a)$$

From (A.13) one can immediately see that

$$\gamma''_{r,\mathrm{cyl}}(0^+,\theta)=2D\sin\theta\cos\theta/V. \quad (A.14)$$

Consequently, the angularity is different from zero when the edges are completely seen, *i.e.* $\theta\neq 0$, π and $\theta\neq\pi/2$. Similarly, when condition (A.9) is obeyed, the finite discontinuity is

$$\gamma''_{r,\mathrm{cyl},\Delta}(H/\cos\theta,\theta)=-[8\sin\theta\cos\theta/\pi HD]\times[1-(H\tan\theta/D)^2]^{1/2}. \quad (A.15)$$

By contrast, when

$$t\sin\theta=D \quad\text{and}\quad \theta\geq\theta_0\equiv\arctan(D/H), \quad (A.16)$$

from (A.15) one sees that the discontinuity is a divergent one. Moreover, for positive t's, the negativeness of $\gamma'_{r,\mathrm{cyl}}(t,\theta)$ as well as the positiveness of $\gamma''_{r,\mathrm{cyl}}(t,\theta)$, following from the convexity of the particle, appear evident from (A.11) and (A.13).*

Unfortunately, the evaluation of the peak profile, through the Fourier transform of (A.7), is not possible in a closed explicit form and must be done in a numerical way. We have considered the case $H/D=1$ and Figs. 2(a), (b) illustrate the results for the angles $\theta=\pi/3$ and $\theta=\pi/6$.

(c) *Cubic particle*

This case does not offer new insights and thus it will be discussed very briefly. After having chosen the origin at one of the cube vertex and the axes along the edges coming out from the latter, let (s_1, s_2, s_3) and s_M denote respectively the three components of $\hat{\mathbf{s}}_{0r}$ and the maximum of the latter absolute values, *i.e.* $s_M=\max(|s_1|,|s_2|,|s_3|)$. The origin of the cube translated by $t\hat{\mathbf{s}}_{0r}$ will have coordinates (ts_1, ts_2, ts_3).

* It is not difficult to show that in the case of a hollow cylinder, whose radii are R_1 and R_2, the second derivative of the oSPF, with the stick oriented along one of the cylinder diameters, becomes negatively divergent as $t\to(R_1+R_2)^-$.

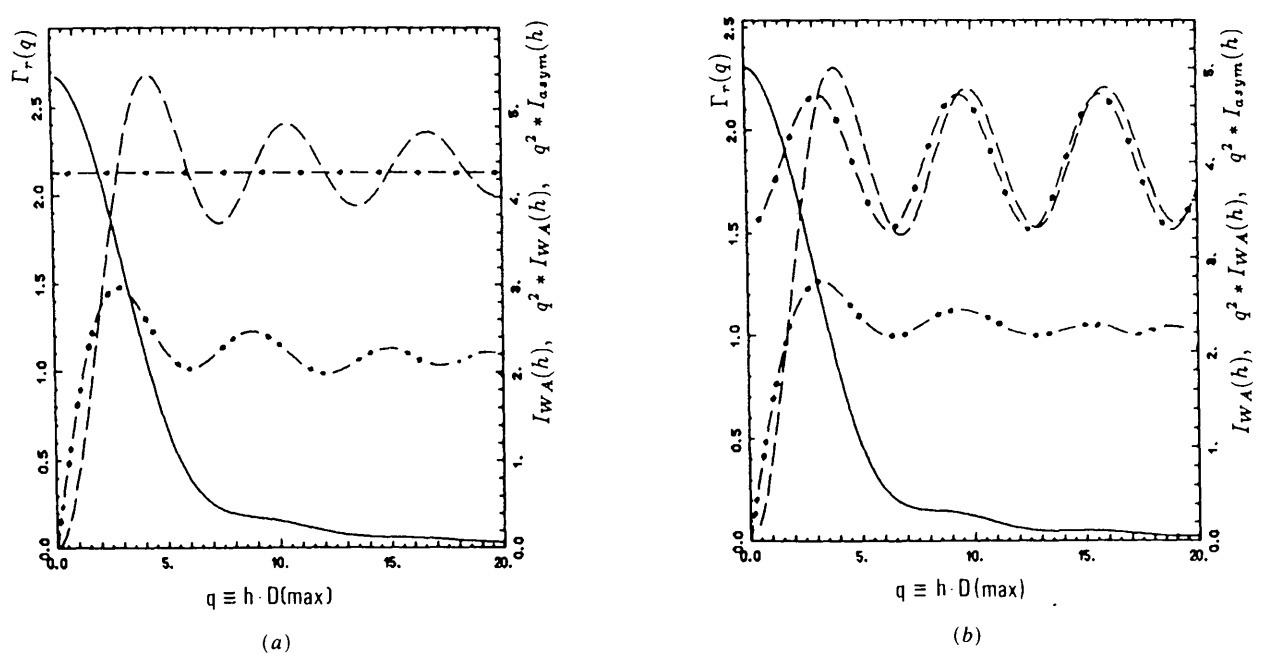

Fig. 2. The meaning of the curves is as in Fig. 1 but the particle is a right circular cylinder having height equal to the diameter D and thus, from (A.9), $\theta_0=\pi/4$. Two different angular orientations ($\equiv\theta$) of the cylinder axis with respect to the reflexion direction are considered. (a) $\theta=\pi/3$. In this case, $\theta>\theta_0$, $D_{\max}=2D/3^{1/2}$ (see equation A.7) and from equation (A.11) one knows that the first-order derivative of the correlation function is continuous and thus the leading asymptotic term will not oscillate. In this way, similarly to the case of the sphere, we have a horizontal Porod plateau (the dotted-dashed line) while the Porod plot of the intensity (the broken curve) shows oscillations of decreasing amplitude around this line. Since the cylinder has sharp edges visible along the considered reflexion direction, the angularity is non null, as one can see from (A.14). The double-dotted dashed curve shows that the exact value of the angularity, 1·103, is approached more quickly than in the former case. (b) $\theta=\pi/6$ and $D_{\max}=2D/3^{1/2}$. Since $\theta<\theta_0$, we have a discontinuous first-order derivative of $\gamma_r(t)$. The discontinuity value is given by (A.10). Then, from (32), the leading asymptotic term, once it has been multiplied by q^2, will be the sum of a constant and of an oscillatory term. Once more this contribution is represented by the dotted-dashed curve. From the figure it also appears clear how the plot of $q^2 I_{\mathrm{WA},r,\mathrm{cyl}}(h)$, *i.e.* the dashed line, becomes closer to the former curve. As in (a), the double-dotted dashed curve shows a rather fast approach to the exact angularity value (1·103).

With L denoting the edge length, the overlapping volume will be $\prod_{i=1}^{3}(L-|ts_i|)$ and the oSPF of the cube is

$$\gamma_{r,\mathrm{cub}}(t,\hat{\mathbf{s}}_{0r})=\begin{cases}\prod_{i=1}^{3}(1-|ts_i/L|) & \text{when } |t|\le L/s_M\\ 0 & \text{elsewhere,}\end{cases}\qquad (A.17)$$

where

$$L/s_M\equiv D_{\max}\equiv\min(L/|s_1|,\,L/|s_2|,\,L/|s_3|).\qquad (A.17a)$$

From the geometry of the cube and from (22) one deduces that

$$\gamma'_{r,\mathrm{cub}}(0^+,\hat{\mathbf{s}}_{0r})=-L^2(|s_1|+|s_2|+|s_3|)/L^3$$
$$=-\sum_{i=1}^{3}|s_i|/L.\qquad (A.18)$$

Moreover, for any $\hat{\mathbf{s}}_{0r}$, the derivative of the oSPF has a finite discontinuity at L/s_M. For this t value, in fact, we have a partial superposition of that pair of the cube faces whose unit normal is closer to $\hat{\mathbf{s}}_{0r}$.* The discontinuity is

$$\gamma'_{r,\mathrm{cub},\Delta}(L/s_M,\hat{\mathbf{s}}_{0r})=(s_M/L)\prod_{i=1}^{3}{}'(1-|s_i|/s_M),\qquad (A.19)$$

where the prime on the product symbol means that we have to neglect the index value which yields a null factor.

Turning to the second-order derivative we have both a non-null angularity and a finite discontinuity. One finds in fact that

$$\gamma''_{r,\mathrm{cub}}(0^+,\hat{\mathbf{s}}_{0r})=2\sum_{i<j=1}^{3}|s_is_j|/L^2\qquad (A.20)$$

$$\gamma''_{r,\mathrm{cub},\Delta}(L/s_M,\hat{s}_{0r})$$
$$=-2(s_M/L^2)\{|s_i|(1-|s_j|/s_M)+i\leftrightarrow j\},\qquad (A.21)$$

where $i\neq j\neq M$ and $i,j,N\in\{1,2,3\}$. The peak profile can be straightforwardly evaluated and one finds

$$I_{\mathrm{WA,cub}}(h,\hat{\mathbf{s}}_{0r})$$
$$=\frac{2L}{s_M}\left\{\frac{A}{q^2}+B\frac{\cos q}{q^2}-2C\frac{\sin q}{q^3}-6D\frac{1-\cos q}{q^4}\right\}\qquad (A.22)$$

with

$$q\equiv hL/s_M,\qquad A\equiv 1+E,$$
$$B\equiv -1+E-D,\qquad C\equiv E-2D,\qquad (A.23)$$
$$D\equiv|s_is_j|/s_M^2,\qquad E\equiv(|s_i|+|s_j|)/s_M.$$

To check (32) and (34) is rather simple. For the latter in particular it is convenitent to integrate by parts the contribution due to the last term in (A.22) and then one has to recall that $\int_0^\infty x^{-1}\sin x\,dx=\pi/2$. Fig. 3 shows the peak profile and allows one to see that, as in the other cases, the onset of the asymptotic regime takes place, roughly, at $q\simeq 2\pi$.

* By closer we mean that the absolute value of their scalar product is closer to one than for the remaining two pairs of faces.

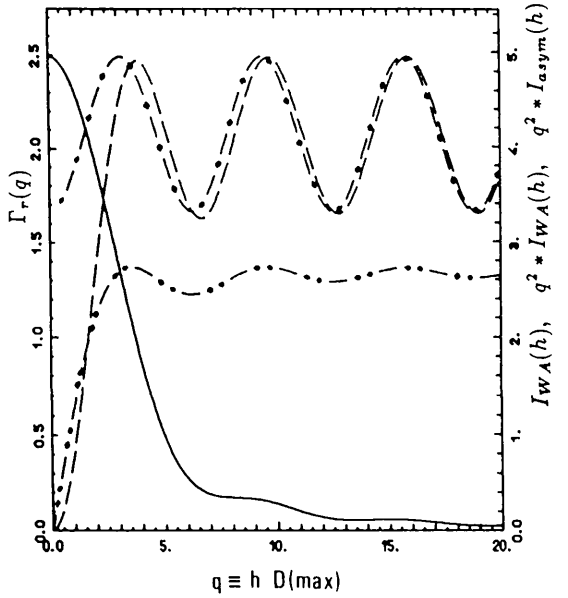

Fig. 3. The curves, with the same meaning as in Figs. 1 and 2, are relevant to a cube having edges of length L and oriented along the axes. The reflexion orientation is characterized by the following polar angles: longitude $\varphi=\pi/3$, latitude $\theta=\pi/6$. In this case $D_{\max}=2L/3^{1/2}$ and the angularity is 1·40.

References

ALLEGRA, G. (1982). *Acta Cryst.* **A38**, 863-868.

BALE, H. D. & SCHMIDT, P. W. (1984). *Phys. Rev. Lett.* **53**, 596-599.

BENEDETTI, A., FAGHERAZZI, G., PINNA, F. & POLIZZI, S. (1990). *J. Mater. Sci.* In the press.

CICCARIELLO, S. (1985). *Acta Cryst.* **A41**, 560-568.

CICCARIELLO, S. (1989). *Acta Cryst.* **A45**, 86-99.

CICCARIELLO, S. & BENEDETTI, A. (1985). *J. Appl. Cryst.* **18**, 219-229.

CICCARIELLO, S., GOODISMAN, J. & BRUMBERGER, H. (1988). *J. Appl. Cryst.* **21**, 117-128.

DEBYE, P., ANDERSON, H. R. & BRUMBERGER, H. (1957). *J. Appl. Phys.* **28**, 679-683.

DELHEZ, R., DE KEIJESER, TH. H. & MITTEMEIJER, E. J. (1982). *Z. Anal. Chem.* **312**, 1-16.

ENZO, S., FAGHERAZZI, G., BENEDETTI, A. & POLIZZI, S. (1988). *J. Appl. Cryst.* **21**, 536-542.

FEDOROVA, I. S. & SCHMIDT, P. W. (1978). *J. Appl. Cryst.* **11**, 405-411.

GUINIER, A. (1963). *X-ray Diffraction.* San Francisco: Freeman.

INO, T. & MINAMI, N. (1979). *Acta Cryst.* **A35**, 163-170.

JONES, D. S. & KLINE, M. (1958). *J. Math. Phys. (Cambridge, Mass.)*, **37**, 1-28.

LUZZATI, V., WITZ, J. & NICOLAIEFF, A. (1961). *J. Mol. Biol.* **3**, 367-378.

MILLER, A. & SCHMIDT, P. W. (1962). *J. Math. Phys. (NY)*, **3**, 92-96.

POROD, G. (1965). *Small-Angle X-ray Scattering*, edited by H. BRUMBERGER, pp. 1-16. New York: Wiley.

TCHOUBAR, D. & MÉRING, G. (1969). *J. Appl. Cryst.* **2**, 128-139.